(Received 3 January 2026, Accepted 21 February 2026, Scheduled 18 March 2026)

Design and Experimental Validation of Linear to Circular Polarization Converter for Point to Point THz Communication

Murtaza Waheed[1,*], Javid A. Ganie[1], Mingyan Zhong[2], Qusay Al-Taai[2], Kushmanda Saurav[1], and Chong Li[2]

[1]*Indian Institute of Technology Jammu, Jammu and Kashmir 181221, India*
[2]*School of Engineering, University of Glasgow, Glasgow G12 8QQ, United Kingdom*

ABSTRACT: This letter presents a compact, low-profile single-substrate transmissive linear-to-circular polarization (LCP) converter designed and experimentally validated for point-to-point THz communication bands. The proposed LCP converter consists of an H-shaped gold metallic pattern deposited on both sides of a 100 µm-thick fused silica substrate. The LCP converter operates within the 0.225–0.307 THz frequency band, achieving a simulated 3-dB axial ratio bandwidth of 30.8% in simulation. Owing to its wide axial ratio bandwidth, the proposed design is a promising candidate for point-to-point THz communication applications. The performance of the proposed converter is verified through surface current distribution, which explains the occurrence of Hyugen's response and equivalent circuit model. The proposed converter exhibits a measured 3-dB axial-ratio bandwidth of 27.8% in the frequency band 0.229–0.303 THz. The simple geometry and single-substrate implementation, with a thin profile and wide 3-dB axial ratio bandwidth, make the proposed design suitable for practical deployment scenarios.

1. INTRODUCTION

Terahertz (THz) waves, typically spanning from 0.1 to 10 THz, have gained significant attention for high-data rate wireless communication, spectroscopy, sensing, and imaging applications [1, 2]. The IEEE 802.15.3d standard allocates the 252–325 GHz band for point-to-point THz links supporting ultra-high-speed data transmission [3]. To harness the full potential of THz waves, the precise control of their amplitude, phase, and polarization is crucial [4]. Among them, polarization control is particularly important, as it enhances signal quality, mitigates multipath interference, and enables polarization-sensitive detection [5, 6].

Linear-to-circular polarization (LCP) conversion is especially vital since most THz sources inherently emit linearly polarized waves. Efficient LCP conversion is essential for advanced communication, sensing, and imaging systems. Conventional birefringent-crystal waveplates [7, 8] have been widely used for polarization conversion, but they suffer from bulky structures, narrow bandwidth, high material losses, and limited integration compatibility at THz frequencies.

In recent years, metasurfaces composed of subwavelength resonators have emerged as compact, lightweight, and broadband alternatives for polarization control [9–12]. By manipulating the phase and amplitude of orthogonal wave components, metasurface-based converters achieve high conversion efficiency. Although both reflection [13, 14] and transmission type converters have been studied, reports on transmissive LCP converters at THz frequencies remain limited. These devices are particularly desirable for the integration with optical components and THz antennas but are more challenging to design than their reflective counterparts.

Several THz transmission-type LCP converters have been reported. In [15], a multilayer dog-bone shaped design using two dielectric substrates and three metallic layers achieved a 26% axial ratio (AR) bandwidth with 75% transmission efficiency (TE). A similar multilayer configuration in [16] employing metallic patch resonators achieved the widest AR bandwidth of 53% and 70% TE. A more compact single substrate layer design [17] reduced electrical thickness but offered only a 26.2% AR bandwidth and 60% TE. In [18], a single substrate layer converter is proposed with simplified fabrication but yielding only 12.8% AR bandwidth with improved TE of 80%.

Microwave LCP converters are widely reported in the literature [19–24] because of their relatively large dimensions, which makes fabrication, measurement, and characterization easier. Extending the microwave LCP converters to THz frequencies remains a significant challenge. In addition to fabrication, modeling, and measurement constraints, direct geometric scaling becomes impractical, as higher frequencies demand extremely small feature sizes, very low tolerances, and careful control of material dispersion and losses. Consequently, substantial design optimization and advanced characterization techniques are required to achieve reliable performance at THz frequency bands. Therefore, there remains significant scope for developing single-substrate-layer and transmission-type LCP converters operating in the THz band that offer wideband CP with high TE.

* Corresponding author: Murtaza Waheed (murtazawaheed13@gmail.com).

In this work, a transmissive metasurface-based LCP converter operating in the THz range is presented. The design employs H-shaped metallic resonators patterned on both sides of the substrate and achieves a 3-dB axial ratio (AR) bandwidth of 0.225–0.307 THz, corresponding to a relative bandwidth of 30.8%.

The key contributions highlighting the novelty of the proposed work with respect to the reported THz converters are summarized as follows:

1. The proposed design features a compact profile with a normalized thickness of just 0.075λ, which is considerably thinner than those reported in [15–18]. Moreover, its implementation on an optically transparent substrate makes it well-suited for transparency-based applications.

2. The design achieves a 3-dB AR bandwidth of 30.8%, outperforming existing converters [15, 17, 18], except [16].

3. A systematic design evolution from rectangular to H-shaped metallic patterns has been studied to analyze the enhancement in 3-dB AR bandwidth obtained through progressive geometric modification.

4. The surface current distribution has been studied to analyze the excitation of Huygens resonance in both the X and Y polarizations of the incident wave, which is eventually responsible for wideband linear polarization (LP) to CP conversion with a good transmission efficiency.

5. The operating mechanism of the proposed structure is validated using an equivalent circuit model (ECM), whose magnitude and phase responses exhibit excellent agreement with full-wave simulation results.

6. The performance of the converter is experimentally validated in the 0.20–0.32 THz range using a fabricated prototype comprising 21×21 unit cells.

The combination of wide bandwidth and structural simplicity makes the proposed LCP converter suitable for integration into THz wireless communication, imaging, and sensing applications.

2. WORKING PRINCIPLE

When a linearly polarized incident wave impinges on the metasurface, the transmitted electric field can be decomposed into two orthogonal components along the x- and y-directions, characterized by the transmission coefficients T_{xx} and T_{yy}, respectively.

For efficient linear-to-circular polarization conversion, the magnitudes of the co-polarized transmission coefficients must be equal, i.e.,

$$|T_{xx}| = |T_{yy}|. \tag{1}$$

In addition, a phase difference of $\pm 90^\circ$ between the transmitted orthogonal components is required, which can be expressed as

$$\Delta\phi = \phi_x - \phi_y = \pm 90^\circ, \tag{2}$$

where ϕ_x and ϕ_y denote the transmission phases corresponding to T_{xx} and T_{yy}, respectively.

Under these conditions, the superposition of the two orthogonal transmitted fields results in a circularly polarized wave. Thus, by properly designing the geometry of the metasurface unit cell, the required amplitude balance and phase difference are achieved over the desired operating frequency band, enabling efficient transmission-type LCP conversion.

3. UNIT CELL DESIGN AND PERFORMANCE PARAMETERS

A systematic design evolution, progressing from a rectangular to an H-shaped metallic pattern, was carried out to investigate the enhancement in the 3-dB axial ratio (AR) bandwidth achieved through gradual geometric modifications. The evolution of the proposed unit cell, along with the corresponding simulated results, is illustrated in Fig. 1. In the initial stage, a simple rectangular metallic strip was patterned on both the top and bottom surfaces of a 100 µm thick fused silica substrate ($\varepsilon_r = 3.75$, $\tan\delta = 0.0004$), as shown in Fig. 1(a). In the second stage, two vertical rectangular strips were introduced on either side of the substrate, modifying the geometry of the first stage, as depicted in Fig. 1(b). In the final stage, the horizontal metallic strips were extended on both sides, resulting in an H-shaped metallic pattern on the top and bottom layers of the substrate, as illustrated in Fig. 1(c). All simulations were carried out in Computer Simulation Technology (CST) Microwave Studio with periodic boundary conditions in the x- and y-directions and open (add space) boundary conditions in the z-direction. A normally incident linearly polarized plane wave excitation was applied using Floquet ports in $+z$ and $-z$ directions in order to obtain transmission and reflection coefficients.

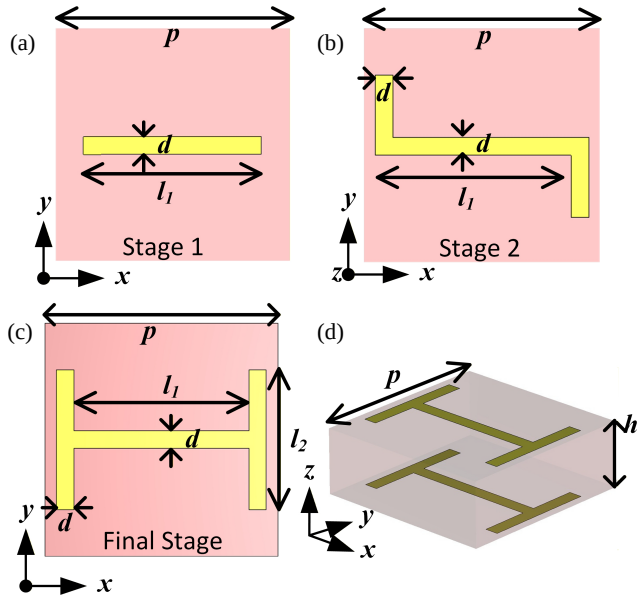

FIGURE 1. Design evolution (a) stage 1, (b) stage 2, (c) final stage and (d) perspective view of the proposed LCP converter with geometric parameters ($p = 400$ µm, $h = 100$ µm, $l_1 = 300$ µm, $l_2 = 240$ µm, $d = 30$ µm).

For an ideal LCP converter, the transmission magnitudes of the orthogonal linearly polarized components must be equal and close to unity, and the phase difference between them must be 90°. Figs. 2(a) and (b) present the magnitude and phase dif-

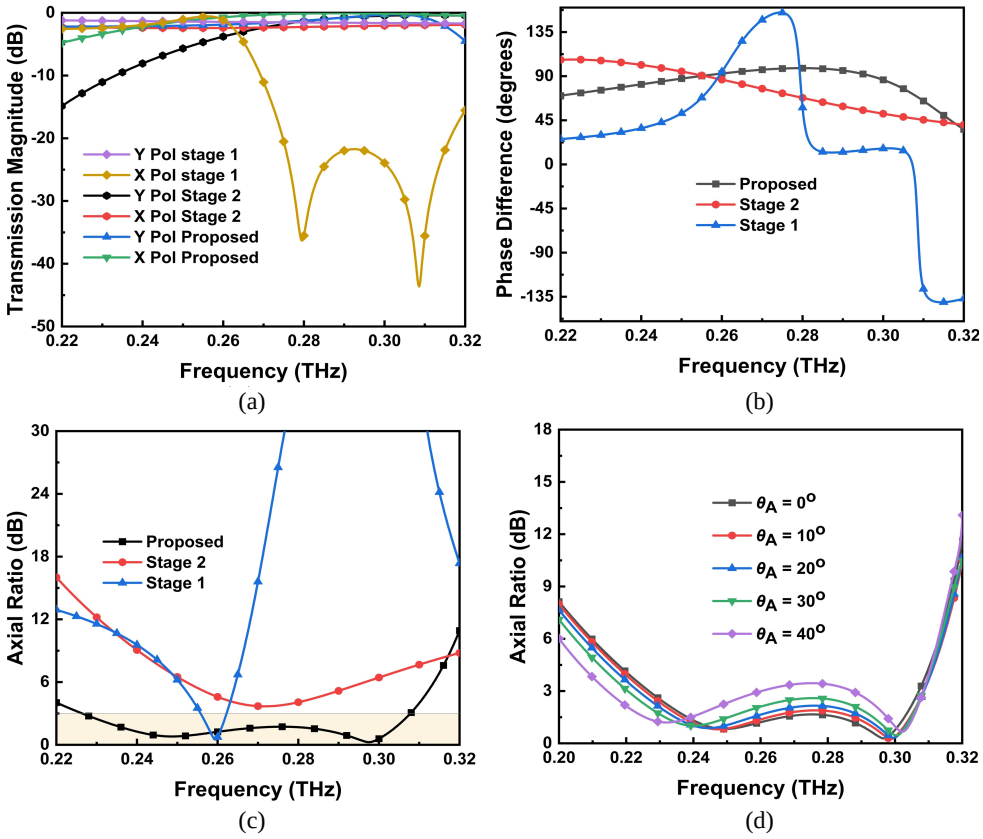

FIGURE 2. Simulated transmission (a) magnitude, (b) phase difference, (c) axial ratio for the different design stages of the proposed LCP converter. (d) Simulated axial ratio under oblique incidence for the proposed LCP converter.

ference of transmission coefficients, respectively for all stages under both X- and Y-polarizations.

In stage 1, the required magnitude and phase response for LCP conversion was achieved for a narrow band 0.255–0.262 THz while stage 2 shows that the transmission magnitude above -2.22 dB was achieved from 0.26 to 0.319 THz under both X- and Y-polarizations, but the required phase difference of $90 \pm 20°$ was not achieved. For the final stage, the simulation results show efficient transmission with a phase difference of $90 \pm 20°$ over the frequency range of 0.225–0.307 THz, as shown in Figs. 1(c) and (d), respectively.

The simulated axial ratio of all design stages under normal incidence is presented in Fig. 2(c). The axial ratio is calculated using (3).

$$\mathrm{AR} = \sqrt{\frac{T_{xx}^2 + T_{yy}^2 + \sqrt{T_{xx}^4 + T_{yy}^4 + 2T_{xx}^2 T_{yy}^2 \cos(2\Delta\phi)}}{T_{xx}^2 + T_{yy}^2 - \sqrt{T_{xx}^4 + T_{yy}^4 + 2T_{xx}^2 T_{yy}^2 \cos(2\Delta\phi)}}} \quad (3)$$

As observed, stage 1 exhibits a 3-dB AR bandwidth from 0.255 to 0.262 THz, and stage 2 exhibits AR above 3.6 dB, whereas the proposed configuration achieves a significantly wider 3-dB AR bandwidth ranging from 0.225 to 0.307 THz. The oblique incidence AR performance is shown in Fig. 2(d), and the proposed LCP converter demonstrates stable polarization conversion with a 3-dB AR bandwidth of 30.8% (0.225–0.307 THz) maintained up to a 30° incidence angle. The surface current distribution on the proposed LCP converter is shown in Fig. 3. For the X-polarization case, the surface currents on the top and bottom metallic layers (denoted as $\mathbf{J}_1$ and $\mathbf{J}_2$ in Fig. 3(a) flow in-phase at the instant t_{x1}, forming an electric resonance and producing an equivalent current $\mathbf{J}_e$ directed along the x-axis. At the instant t_{x2}, the currents on the two layers flow in opposite directions ($+x$ and $-x$) as shown in Fig. 3(b), resulting in a magnetic resonance and generating an equivalent magnetic current $\mathbf{J}_m$ along the y-axis, thus providing a Huygens resonance.

Similarly, under Y-polarized incidence, at the instant t_{y1}, the top and bottom layer currents flow in-phase along the y-direction, giving rise to an electric resonance, as shown in Fig. 3(c). At t_{y2}, the currents become out-of-phase, while some small in-phase current components are still present, leading primarily to a comparatively weaker magnetic response. Due to the relatively weaker coupling between the electric and magnetic modes for this polarization, as shown in Fig. 3(d), the Y-polarized case exhibits partially in-phase and out-of-phase current behavior, resulting in a weaker Huygens resonance.

Overall, the X-polarization demonstrates a stronger Huygens response than the Y-polarization. These stronger resonances lead to improved transmission performance for the X-polarized wave. Due to both electric and magnetic resonances in the proposed LCP converter, a wide operational bandwidth is achieved.

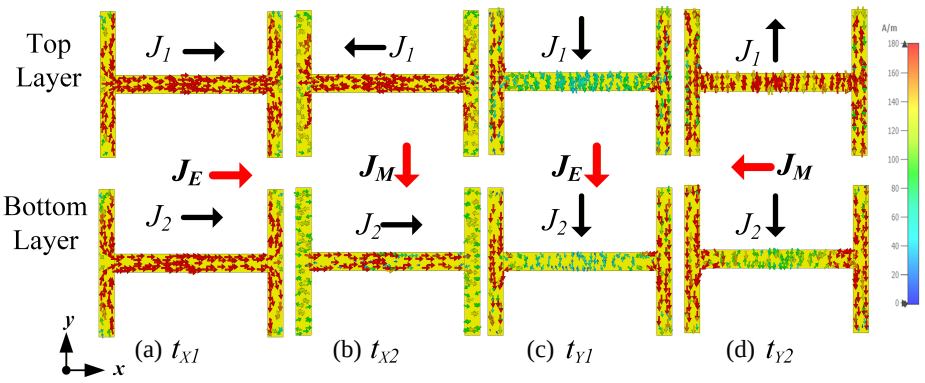

FIGURE 3. Surface current distribution on the proposed LCP converter at Huygens resonance frequencies: (a) electric response and (b) magnetic response along x-polarization at 0.270 THz. (c) Electric response and (d) magnetic response along y-polarization at 0.227 THz.

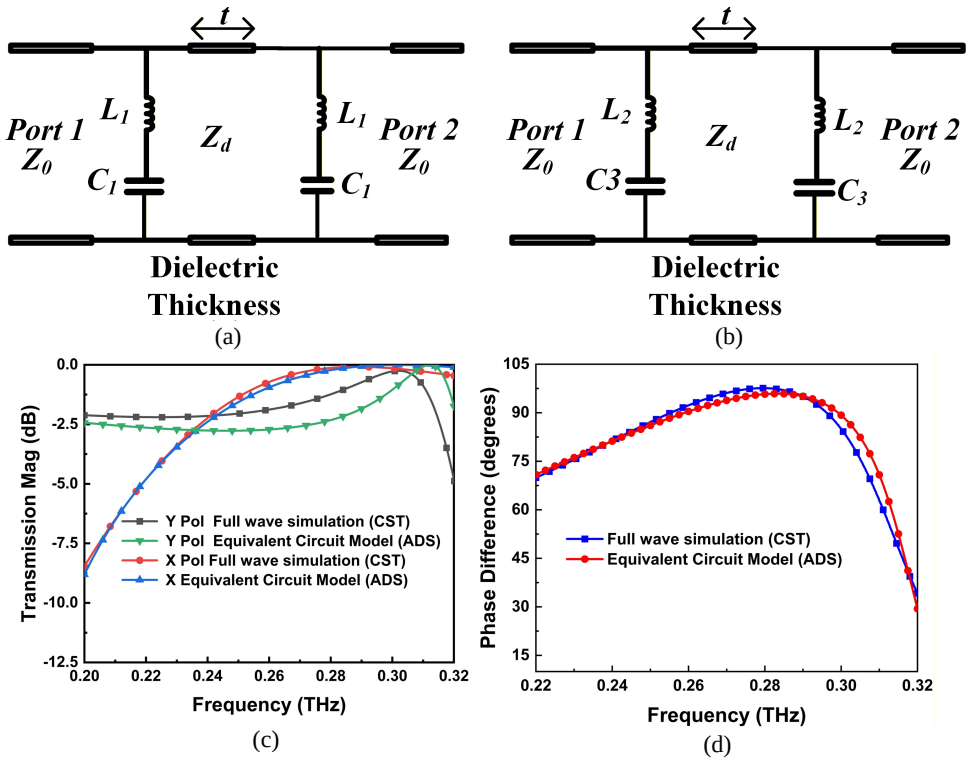

FIGURE 4. Equivalent circuit model with component values of the proposed LCP converter under (a) Y-polarization and (b) X-polarization of incident wave ($Z_0 = 377\,\Omega$, $Z_d = 194.6\,\Omega$, $L_1 = 257$ pH, $L_2 = 412$ pH, $C_1 = 0.77$ fF, $C_3 = 6.42$ fF. (c) Transmission magnitude, and (d) phase difference comparison between ECM and full-wave simulation results for the proposed LCP converter.

4. EQUIVALENT CIRCUIT MODEL

The equivalent circuit model (ECM) of the proposed converter was developed using the advanced design system (ADS) circuit simulator and is presented in Figs. 4(a) and 4(b) for the Y- and X-polarizations, respectively. The circuit topologies for the Y and X polarizations are identical; however, the corresponding lumped component values differ due to the anisotropic nature of the proposed unit-cell geometry along the X- and Y-polarization directions. The ECM for Y-polarization is modelled as a two-port network with its impedance matched to the free space impedance. It comprises two identical series branches of a capacitor C_1 and an inductor L_1, parallel to each other and separated by a dielectric layer. L_1 corresponds to the H-shaped metallic pattern on both sides of the substrate, and C_1 corresponds to the gap between the adjacent unit cells in both x and y directions. The dielectric layer is modelled as a transmission line having the length equal to the dielectric substrate thickness t and characteristic impedance Z_d, given by $Z_d = Z_0/\sqrt{\epsilon_r}$. The initial values of lumped components are derived using Equations (4) and (5) [25].

$$L = \frac{\mu_0 P_{x/y}}{2\pi} \ln\left[\left(\sin\left(\frac{\pi w}{2P_{x/y}}\right)\right)^{-1}\right] \tag{4}$$

$$C = \frac{2\varepsilon_0 \varepsilon_{eff} P_{x/y}}{\pi} \ln\left[\left(\sin\left(\frac{\pi g}{2P_{x/y}}\right)\right)^{-1}\right] \tag{5}$$

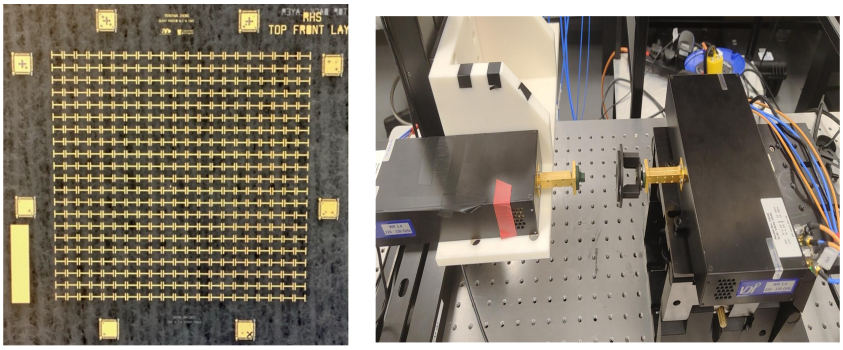

(a) (b)

FIGURE 5. (a) Photograph of fabricated prototype, (b) measurement setup of the proposed LCP converter.

$P_{x/y}$, w, and g represent the periodicity (p), strip width (d), and the gap between adjacent unit cells in the x- and y-directions, respectively. The equivalent circuit was modeled in the ADS circuit simulator, and the initial lumped-element parameters derived from (1) and (2) were subsequently optimized.

For X-polarization, C_1 and L_1 are replaced by C_3 and L_2, respectively. Figs. 4(c) and (d) present the transmission magnitudes and phase difference of the proposed LPC converter obtained from the equivalent circuit model and full-wave simulations. The transmission magnitudes for both X- and Y-polarized components and their phase difference obtained from the ECM and full-wave simulations show close agreement, with only minor discrepancies. These discrepancies arise from differences in modeling approaches: CST solves the full-wave Maxwell equations and accounts for distributed electromagnetic effects, higher-order modes, substrate dispersion, and coupling, whereas the ADS equivalent circuit model relies on lumped-element approximations derived from simplified analytical expressions. Consequently, parasitic effects, radiation losses, and frequency-dependent material properties are not fully captured in the ECM.

5. FABRICATION AND MEASUREMENT RESULTS

The proposed polarizer was fabricated using a photolithography-based process, offering excellent scalability for large-area production. The same fabrication procedure was applied to both sides of a 100 µm-thick fused silica substrate, enabling the realization of a double-layer structure, and the fabricated prototype consisting of 21×21 unit cells is illustrated in Fig. 5(a). Following thorough surface cleaning to enhance photoresist adhesion, a bi-layer photoresist stack consisting of LOR10 and S1818 was spin-coated onto the substrate at 500RPM for 30 seconds. Each side of the substrate underwent a sequence of standard microfabrication steps, including surface preparation, resist coating, soft baking, ultraviolet (UV) exposure, development, metal deposition, and lift-off. Double-sided patterning required precise alignment between the two patterned layers, which was achieved using front-side alignment markers that remained visible through the transparent substrate during backside processing. The array patterns were defined using an optical mask aligner (MA6). After UV exposure, the samples were developed in MF319 solution for 150 s, followed by rinsing under running deionized water for 6 min. Subsequently, a Ti/Au metal stack with thicknesses of 20 nm and 330 nm, respectively, was deposited using plasma-enhanced chemical vapor deposition (PECVD) to form the double split-ring resonator (DSRR) structures. During this step, alignment markers were also patterned to facilitate accurate backside fabrication. To ensure reliable pattern transfer and structural integrity, strict process control was implemented throughout the fabrication process. Common fabrication challenges, including resist delamination, incomplete lift-off, and substrate warping, were mitigated by optimizing critical parameters, such as the baking temperature (150°C), spin-coating conditions (5000 rpm for 30 s for LOR10 and 4000 rpm for 30 s for S1818 resist), and solvent processing conditions.

The measurement of the proposed LCP converter was carried out using a pair of standard gain horns from Flann Microwave (32240) operating in the 0.217–0.330 THz band. The characterization was carried out using two 220–330 GHz frequency extenders from Virginia Diodes Inc. (VDI), which were used to extend the signal from an Agilent N5224A PNA. The complete measurement setup is illustrated in Fig. 5(b).

The measured transmission magnitude and corresponding phase differences are presented in Fig. 6(a) and Fig. 6(b), respectively. The results indicate that the proposed LCP converter exhibits an insertion loss of less than 3-dB within the frequency range of 0.230–0.312 THz for both x- and Y-polarizations. Furthermore, a phase difference of $90° \pm 20°$ is observed across the 0.220–0.307 THz range, validating the quarter-wave behavior required for circular polarization conversion. The measured axial ratio of the proposed design is shown in Fig. 6(b), and a 3-dB axial ratio bandwidth of 28.25% is achieved in the frequency range of 0.229–0.303 THz. The slight reduction in the measured bandwidth is mainly attributed to fabrication and measurement tolerances, such as metal thickness variations, substrate parameter uncertainties, and minor alignment errors between the top and bottom metallic patterns.

Another important performance evaluation parameter is the extinction ratio (ER), which indicates the quality and purity of the CP wave. The ER of the proposed polarization converter

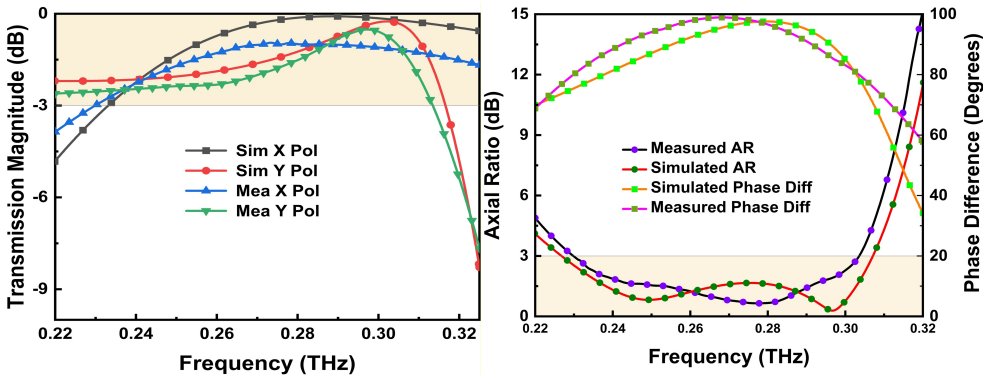

FIGURE 6. (a) Measured transmission magnitudes, (b) phase difference and axial ratio, extinction ratio and ellipticity, transmission efficiency of the proposed LCP converter.

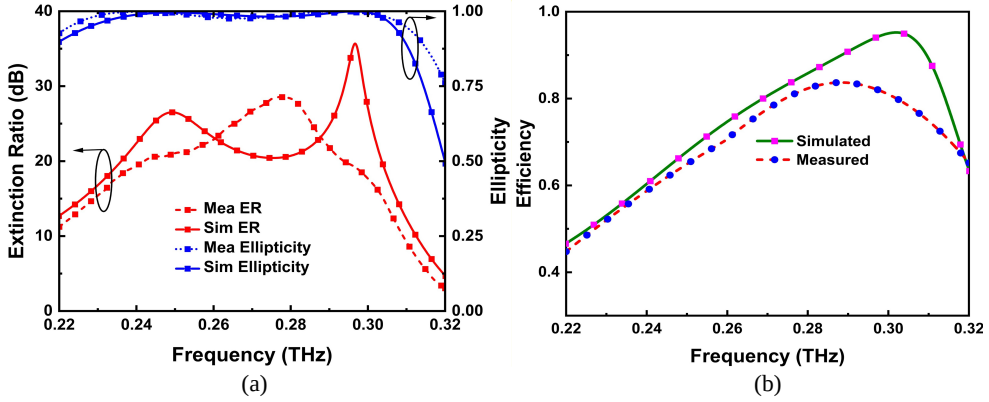

FIGURE 7. (a) Simulated and measured: ER and ellipticity, (b) efficiency of proposed LCP converter.

is calculated from AR using (6) and is presented in Fig. 7(a), demonstrating values exceeding 15 dB within the frequency range of 0.227 to 0.307 THz.

$$\mathrm{ER} = \left(\frac{\mathrm{AR}+1}{\mathrm{AR}-1}\right)^2 \tag{6}$$

For an LCP converter, ellipticity and transmission efficiency are key performance indicators, which can be evaluated using the Stokes parameters [15]:

$$S_0 = |S_{21}^{xx}|^2 + |S_{21}^{yy}|^2 \tag{7}$$
$$S_1 = |S_{21}^{xx}|^2 - |S_{21}^{yy}|^2 \tag{8}$$
$$S_2 = 2|S_{21}^{xx}||S_{21}^{yy}|\cos\Delta\phi \tag{9}$$
$$S_3 = 2|S_{21}^{xx}||S_{21}^{yy}|\sin\Delta\phi \tag{10}$$

The ellipticity γ is defined as

$$\gamma = \frac{S_3}{S_0} \tag{11}$$

where $\gamma = 1$ denotes an ideal left-handed circularly polarized wave, and $\gamma = -1$ denotes an ideal right-handed circularly polarized wave. The ellipticity plot is shown in Fig. 7(a). The ellipticity is close to $+1$, indicating that the proposed LCP converter transforms the incident linearly polarized wave into a left-handed circularly polarized (LHCP) wave.

Another key performance evaluation parameter is TE, which can be evaluated using the Stokes parameters and is calculated using (12).

$$\mathrm{TE} = \frac{1}{2}(S_0) \tag{12}$$

The TE of the proposed LCP converter is shown in Fig. 7(b). The TE greater than 60% in the frequency range of 0.24–0.32 THz is obtained in the measurement, with the peak simulated and measured TE of 94% at 0.305 THz and 85% at 0.288 THz, respectively. The slight deviation between simulated and measured transmission efficiencies is due to the fabrication and measurement tolerances. These performance parameters provide a comprehensive method for evaluating the polarization conversion performance of a metasurface-based LCP converter.

The comparison of the proposed LCP converter with existing designs is summarized in Table 1. The proposed structure demonstrates several advantages over prior works, which are listed below:

- The proposed design exhibits a compact profile, with a normalized thickness of 0.075λ, which is significantly lower than the designs reported in [15–18]. Additionally, it is implemented on an optically transparent substrate,

TABLE 1. Comparison of the proposed design with previously reported THz transmission type LCP converters.

Ref.	Thickness λ	Periodicity λ	Substrate layers	Metallic layers	Measured AR BW% < 3-dB	Measured TE %	Angular stability
[15]	0.168	0.454	2	3	26	75	N/A
[16]	0.266	0.369	2	3	53	70	N/A
[17]	0.080	0.23	1	2	26.2	60	N/A
[18]	0.19	0.76	1	2	12.8	80	N/A
Prop.	**0.075**	**0.303**	**1**	**2**	**27.8**	**> 60 84 max**	**30°**

enhancing its suitability for applications requiring transparency.

- It features a simplified architecture comprising a single dielectric substrate with metallic layers printed on both sides, thereby reducing structural complexity in contrast to multilayer configurations utilized in [15, 16].
- The design achieves a 3-dB AR bandwidth of 30.8%, surpassing most existing converters, except for [16], which reports a higher bandwidth at the expense of increased thickness due to multilayer design; hence, there is a trade-off between bandwidth and thickness.

6. CONCLUSION

A compact single-layer transmission-type LCP converter has been designed and experimentally validated for THz communication. The operating principle is verified using an ECM and surface current distribution. The design evolution from a rectangular strip to an H-shaped pattern producing a wideband CP performance is analyzed. The proposed structure operates across the 0.225–0.307 THz band, providing a 3 dB axial ratio bandwidth of 30.8%. Its wide bandwidth and simple design configuration make it a promising candidate for point-to-point THz applications.

ACKNOWLEDGEMENT

This work was supported and funded by

- Anusandhan National Research Foundation (ANRF) under the project titled Design of High Gain Beam Steering Antennas for Millimeter Wave Applications, Grant Number: CRG/2022/002357.
- The UK EPSRC under the grants EP/X017613/1 and EP/W032627/1.

All data supporting this study are provided in full in the FABRICATION AND MEASUREMENT RESULTS section of this paper.

REFERENCES

[1] You, X., C. Fumeaux, and W. Withayachumnankul, "Tutorial on broadband transmissive metasurfaces for wavefront and polarization control of terahertz waves," *Journal of Applied Physics*, Vol. 131, No. 6, 061101, 2022.

[2] Song, H.-J. and T. Nagatsuma, "Present and future of terahertz communications," *IEEE Transactions on Terahertz Science and Technology*, Vol. 1, No. 1, 256–263, Sep. 2011.

[3] IEEE Standards Association, "IEEE Standard for High Data Rate Wireless Multi-Media NetworksAmendment 2: 100 Gb/s Wireless Switched Point-to-Point Physical Layer, IEEE Standard 802.15.3d-2017 (Amendment to IEEE Standard 802.15.3-2016 as amended by IEEE Standard 802.15.3e-2017)," 1–55, 2017.

[4] Tamayama, Y., K. Yasui, T. Nakanishi, and M. Kitano, "A linear-to-circular polarization converter with half transmission and half reflection using a single-layered metamaterial," *Applied Physics Letters*, Vol. 105, No. 2, 021110, 2014.

[5] Cheng, Y. Z., W. Withayachumnankul, A. Upadhyay, D. Headland, Y. Nie, R. Z. Gong, M. Bhaskaran, S. Sriram, and D. Abbott, "Ultrabroadband reflective polarization convertor for terahertz waves," *Applied Physics Letters*, Vol. 105, No. 18, 181111, 2014.

[6] Mo, W., X. Wei, K. Wang, Y. Li, and J. Liu, "Ultrathin flexible terahertz polarization converter based on metasurfaces," *Optics Express*, Vol. 24, No. 12, 13 621–13 627, 2016.

[7] Ji, Y.-Y., F. Fan, X.-H. Wang, and S.-J. Chang, "Broadband controllable terahertz quarter-wave plate based on graphene gratings with liquid crystals," *Optics Express*, Vol. 26, No. 10, 12 852–12 862, 2018.

[8] Wang, J., Y. Li, Z. H. Jiang, T. Shi, M.-C. Tang, Z. Zhou, Z. N. Chen, and C.-W. Qiu, "Metantenna: When metasurface meets antenna again," *IEEE Transactions on Antennas and Propagation*, Vol. 68, No. 3, 1332–1347, Mar. 2020.

[9] Chang, C.-C., Z. Zhao, D. Li, A. J. Taylor, S. Fan, and H.-T. Chen, "Broadband linear-to-circular polarization conversion enabled by birefringent off-resonance reflective metasurfaces," *Physical Review Letters*, Vol. 123, No. 23, 237401, 2019.

[10] Khan, H. Z., J. Zafar, A. Jabbar, *et al.*, "Advancements in metasurfaces for polarization control: A comprehensive survey," *Next Research*, Vol. 2, No. 3, 100407, 2025.

[11] Ako, R. T., W. S. L. Lee, M. Bhaskaran, S. Sriram, and W. Withayachumnankul, "Broadband and wide-angle reflective linear polarization converter for terahertz waves," *APL Photonics*, Vol. 4, No. 9, 096104, 2019.

[12] Ako, R. T., A. Upadhyay, W. Withayachumnankul, M. Bhaskaran, and S. Sriram, "Dielectrics for terahertz metasurfaces: Material selection and fabrication techniques," *Advanced Optical Materials*, Vol. 8, No. 3, 1900750, 2020.

[13] Xu, Z., C. Ni, Y. Cheng, L. Dong, and L. Wu, "Photo-excited metasurface for tunable terahertz reflective circular polarization conversion and anomalous beam deflection at two frequencies independently," *Nanomaterials*, Vol. 13, No. 12, 1846, 2023.

[14] Ako, R. T., W. S. L. Lee, S. Atakaramians, M. Bhaskaran, S. Sriram, and W. Withayachumnankul, "Ultra-wideband tri-layer transmissive linear polarization converter for terahertz waves," *APL Photonics*, Vol. 5, No. 4, 046101, 2020.

[15] Quader, S., R. T. Ako, S. Sriram, C. Fumeaux, and W. Withayachumnankul, "Mechanically reconfigurable polarization converter for terahertz waves," *IEEE Transactions on Terahertz Science and Technology*, Vol. 14, No. 4, 502–509, Jul. 2024.

[16] You, X., R. T. Ako, W. S. L. Lee, M. Bhaskaran, S. Sriram, C. Fumeaux, and W. Withayachumnankul, "Broadband terahertz transmissive quarter-wave metasurface," *APL Photonics*, Vol. 5, No. 9, 096108, 2020.

[17] Wu, J., M. A. S. Syed, L. Qi, X. Tao, J. Yang, and L. Wen, "A double-layer high-transmission terahertz linear-to-circular polarization converter," *Journal of Applied Physics*, Vol. 132, No. 1, 013103, 2022.

[18] Guo, W., P. Tan, J. Wang, L. Li, S. Li, G. Wang, Z. Zhou, and H. Tian, "Multifunctional transmission polarization conversion metasurface based on dislocation-induced anisotropy at the terahertz frequency," *Optics Express*, Vol. 31, No. 2, 2029–2038, 2023.

[19] Dicandia, F. A. and S. Genovesi, "Linear-to-circular polarization transmission converter exploiting meandered metallic slots," *IEEE Antennas and Wireless Propagation Letters*, Vol. 21, No. 11, 2191–2195, Nov. 2022.

[20] Ganie, J. A. and K. Saurav, "A wideband flat gain circularly polarized transmitarray utilizing LP-to-CP converter for Ka-band CubeSat applications," *IEEE Journal on Miniaturization for Air and Space Systems*, Vol. 6, No. 1, 44–52, Mar. 2025.

[21] Zhao, X.-B., F. Wei, J.-Q. Hou, L. Xu, Y. Yang, X. Yang, and N. Wu, "3-D printed conformal dielectric linear-to-circular polarization converters for cylindrical and spherical surfaces," *IEEE Antennas and Wireless Propagation Letters*, Vol. 20, No. 12, 2539–2543, Dec. 2021.

[22] Ganie, J. A. and K. Saurav, "An angularly stable wideband low profile single-layer linear to circular polarization converter for millimeter wave satellite communications," in *2024 18th European Conference on Antennas and Propagation (EuCAP)*, 1–4, Glasgow, United Kingdom, 2024.

[23] He, J., H. Hao, T. Zhang, D. Yin, and Z. Zou, "Linear-to-circular polarization conversion metasurfaces with multibeam for Ka-band satellite applications," *Progress In Electromagnetics Research C*, Vol. 147, 89–97, 2024.

[24] Yuan, L., L. Hou, and Z. Zhang, "Triple-band highly efficient multi-polarization converter based on reflective metasurface," *Progress In Electromagnetics Research M*, Vol. 102, 127–135, 2021.

[25] Wang, H. B., Y. J. Cheng, and Z. N. Chen, "Wideband and wide-angle single-layered-substrate linear-to-circular polarization metasurface converter," *IEEE Transactions on Antennas and Propagation*, Vol. 68, No. 2, 1186–1191, Feb. 2020.